Fast nonlinear regression method for CT brain perfusion analysis

Article *in* Journal of Medical Imaging · June 2016

DOI: 10.1117/1.JMI.3.2.026003

6 authors, including:

Edwin Bennink
University Medical Center Utrecht
49 PUBLICATIONS **628** CITATIONS
SEE PROFILE

Jaap Oosterbroek
University Medical Center Utrecht
11 PUBLICATIONS **43** CITATIONS
SEE PROFILE

Kohsuke Kudo
Hokkaido University
299 PUBLICATIONS **6,291** CITATIONS
SEE PROFILE

Birgitta K Velthuis
University Medical Center Utrecht
377 PUBLICATIONS **11,083** CITATIONS
SEE PROFILE

Journal of Medical Imaging

MedicalImaging.SPIEDigitalLibrary.org

Fast nonlinear regression method for CT brain perfusion analysis

Edwin Bennink
Jaap Oosterbroek
Kohsuke Kudo
Max A. Viergever
Birgitta K. Velthuis
Hugo W. A. M. de Jong

SPIE.

Edwin Bennink, Jaap Oosterbroek, Kohsuke Kudo, Max A. Viergever, Birgitta K. Velthuis, Hugo W. A. M. de Jong, "Fast nonlinear regression method for CT brain perfusion analysis," *J. Med. Imag.* **3**(2), 026003 (2016), doi: 10.1117/1.JMI.3.2.026003.

Fast nonlinear regression method for CT brain perfusion analysis

Edwin Bennink,[a,b,*] Jaap Oosterbroek,[a,b] Kohsuke Kudo,[c] Max A. Viergever,[b] Birgitta K. Velthuis,[a] and Hugo W. A. M. de Jong[a,b]
[a]University Medical Center Utrecht, Department of Radiology, Heidelberglaan 100, 3584CX, Utrecht, The Netherlands
[b]University Medical Center Utrecht, Image Sciences Institute, Heidelberglaan 100, 3584CX, Utrecht, The Netherlands
[c]Hokkaido University Hospital, Department of Diagnostic and Interventional Radiology, N14 W5, Kita-ku, Sapporo 060-8648, Japan

Abstract. Although computed tomography (CT) perfusion (CTP) imaging enables rapid diagnosis and prognosis of ischemic stroke, current CTP analysis methods have several shortcomings. We propose a fast nonlinear regression method with a box-shaped model (boxNLR) that has important advantages over the current state-of-the-art method, block-circulant singular value decomposition (bSVD). These advantages include improved robustness to attenuation curve truncation, extensibility, and unified estimation of perfusion parameters. The method is compared with bSVD and with a commercial SVD-based method. The three methods were quantitatively evaluated by means of a digital perfusion phantom, described by Kudo et al. and qualitatively with the aid of 50 clinical CTP scans. All three methods yielded high Pearson correlation coefficients (>0.9) with the ground truth in the phantom. The boxNLR perfusion maps of the clinical scans showed higher correlation with bSVD than the perfusion maps from the commercial method. Furthermore, it was shown that boxNLR estimates are robust to noise, truncation, and tracer delay. The proposed method provides a fast and reliable way of estimating perfusion parameters from CTP scans. This suggests it could be a viable alternative to current commercial and academic methods. [DOI: 10.1117/1.JMI.3.2.026003]

Keywords: brain; CT perfusion; deconvolution; model; nonlinear regression; stroke.

Paper 15159PRRR received Jul. 28, 2015; accepted for publication May 26, 2016; published online Jun. 16, 2016.

1 Introduction

Computed tomography (CT) perfusion (CTP) imaging of the brain enables rapid diagnosis of ischemic stroke by generating maps of the cerebral blood volume (CBV), cerebral blood flow (CBF), and mean transit time (MTT). Low CBV is an indicator for infarction, whereas tissue at risk shows low CBF but normal CBV. The tissue at risk, or penumbra, may be saved by prompt and correct diagnosis and treatment.

Brain perfusion parameters are commonly derived from a so-called impulse response function (IRF) of the local tissue. The analysis to retrieve this IRF usually involves deconvolution algorithms. Block-circulant singular value decomposition (bSVD) is considered the state-of-the-art deconvolution method because it has been shown to give the most accurate and delay-insensitive estimates.[1] The latter property is important in regions that experience a delayed arrival of the tracer bolus, as is often the case in tissue supplied by collateral flow. It was found that tracer delay-sensitive methods underestimate the CBF and therefore overestimate the final infarct area, whereas the values from delay-insensitive methods correspond well with the infarct area.[2] However, bSVD use is limited to measuring CBV, CBF, and MTT, whereas permeability measurements are of interest for predicting hemorrhagic transformation. bSVD furthermore requires various algorithm parameter settings, such as the method and strength of noise reduction, or the way in which CBV and MTT are calculated.

We propose the use of a model-based, nonlinear regression method with a box-shaped IRF (boxNLR). Although model-based methods for CTP analysis have been proposed before, previous study results turned out to be in favor of model-independent methods, such as bSVD.[3,4] Therefore, SVD-based techniques are currently most frequently used clinically as well as academically. Model-based methods, however, have some advantages over model-independent deconvolution methods. For example, a model-based method provides a unified way of estimating CBF, CBV, MTT, delay, and other perfusion parameters. It is furthermore hypothesized that the boxNLR method will be more robust to time-attenuation curve (TAC) truncation, since the extrapolation of data requires a model. Truncation is a common issue in CTP scans of patients with poor cardiac output or large vessel occlusion, in which case the acquisition times are too short to capture complete TACs.[5,6] The use of model-independent methods in case of truncation is error-prone, since it is unknown what the remainder of the signal would look like, without having any prior knowledge. The sudden cutoffs furthermore introduce spurious frequencies, requiring either strong noise-reduction of the IRF, or a data window that gradually lowers the signal near the cutoff. A model-based method is, however, to a certain extent, able to make an educated guess of the remainder based on the shape of the truncated bolus.

The performance of the model-based method will be evaluated against bSVD and against the delay-insensitive deconvolution method found in the Philips EBW 4.5 Brain Perfusion package (Philips Healthcare, Best, The Netherlands). This

*Address all correspondence to: Edwin Bennink, E-mail: H.E.Bennink@umcutrecht.nl

2329-4302/2016/$25.00 © 2016 SPIE

will be done quantitatively, on the basis of the digital perfusion phantom developed by Kudo et al.,[7] and qualitatively on the basis of 50 clinical CT brain perfusion scans.

2 Methods

2.1 *Digital Perfusion Phantom*

In order to compare the performance of the three methods in quantifying CT brain perfusion, the digital perfusion phantom of Kudo et al. was analyzed. In their publication, the phantom was described in detail.[7] It was used for assessment of bSVD and various other methods for CT and MR perfusion analysis. The phantom consists of 15 slices with 7×7 matrices of tiles with synthetic TACs with uncorrelated Gaussian noise. There are 30 time frames with an interval of 2 s. The standard deviation of the noise is 7.2 HU, which is realistic for e.g., 5-mm thick slices acquired at 80 kVp and 150 mAs/rotation. The arterial input function (AIF) and venous output function (VOF) were modeled as gamma-variate curves. Recirculation was not taken into account.

Each tile represents a patch of uniform tissue and consists of voxels with identical perfusion parameters and equal Gaussian noise level, but different noise realizations. Horizontally in the tiles the MTT was varied (24, 12, 8.0, 6.0, 4.8, 4.0, and 3.4 s), while vertically the tracer delay was varied (0.0 to 3.0 s in steps of 0.5 s). The 15 slices of the phantom have five different CBV values (1.0 to 5.0 mL/100 g) and three types of IRFs (exponential, linear, and box-shaped). The CBF can be determined through the central volume principle: MTT = CBV/CBF.

Prior to analysis, the slices in the phantom were filtered with a two-dimensional (2-D) Gaussian kernel with a standard deviation of 2.5 pixels. No additional filtering was applied.

2.2 *Nonlinear Regression with a Box-Shaped Impulse Response Function*

The proposed method uses a box-shaped model that describes the IRF of the perfused tissue in terms of CBV, MTT, and tracer delay. The convolution of the measured AIF with a computed estimate of the IRF with perfusion parameters $\mathbf{p}$, gives an estimate of the TAC of the tissue

$$\mathrm{TAC}(t) = \mathrm{AIF}(t) \otimes \mathrm{IRF}(t;\mathbf{p}) + \varepsilon(t). \tag{1}$$

This relationship is shown in Fig. 1. The residual term $\varepsilon(t)$ is the difference between the estimated and measured TACs, caused both by measurement noise in $\mathrm{TAC}(t)$ and $\mathrm{AIF}(t)$ and by shortcomings of the model.

Nonlinear regression is used to iteratively adapt the perfusion parameters in the computed IRF (CBV, MTT, and tracer delay) to minimize the mean squared error between the estimated TAC and the measured TAC. Weights might be used in the regression to incorporate additional constraints or prior knowledge, such as the used current-exposure product for a particular time frame. The relatively simple box-shaped IRF enables fast NLR analysis, which is advantageous in time-critical stroke analysis[8]

$$\mathrm{IRF}(t) = F[U(t - t_\Delta)] - U(t - t_\Delta - \mathrm{MTT}). \tag{2}$$

In Eq. (2), $U(t)$ is the unit step function, F is the plasma flow, and t_Δ is the delay in bolus arrival between the AIF and the tissue curve. A similar model, the so called box-modulated transfer function (box-MTF), was introduced by Nambu et al.[9] This model, however, did not include a delay parameter and was thus found to be tracer delay-sensitive. Accordingly, it was outperformed by the bSVD method.[7]

The convolution in Eq. (1), with the IRF as given in Eq. (2), can also be defined in terms of differential equations, i.e., as the solution of

$$\frac{\mathrm{dTAC}(t)}{\mathrm{d}t} = F[\mathrm{AIF}(t - t_\Delta) - \mathrm{AIF}(t - t_\Delta - \mathrm{MTT})] + \frac{\mathrm{d}\varepsilon(t)}{\mathrm{d}t}. \tag{3}$$

When Eq. (3) is integrated, the convolution can be calculated efficiently by sampling the integral of $\mathrm{AIF}(t)$

$$\mathrm{TAC}(t) = F\left(\int_0^{t-t_\Delta} \mathrm{AIF}(\tau)\mathrm{d}\tau - \int_0^{t-t_\Delta-\mathrm{MTT}} \mathrm{AIF}(\tau)\mathrm{d}\tau\right) + \varepsilon(t). \tag{4}$$

An example of a basic implementation of this method has been given as an Appendix to this article. To prevent aliasing artifacts owing to sampling, frequency components in the IRF above the Nyquist frequency should be suppressed. A Bartlett kernel (triangular) with a width of twice the sample interval was therefore used to sample the integral of $\mathrm{AIF}(t)$ and to filter $\mathrm{TAC}(t)$.

The shape of the IRF is the only choice to be made for application of this model-based method in CTP analysis. It should be pointed out that the entire approach described in this section is considered the novelty in this research, rather than solely the box-shaped model in Eq. (2).

2.3 *Block-Circulant Singular Value Decomposition Deconvolution*

The convolution in Eq. (1) can be written as the matrix operation $\mathbf{b} = \mathbf{A}\mathbf{x} + \boldsymbol{\varepsilon}$, where vector $\mathbf{b}$ is $\mathrm{TAC}(t)$, $\mathbf{A}$ is a matrix with zero-padded, circularly shifted versions of $\mathrm{AIF}(t)$ at regular intervals of t, vector $\mathbf{x}$ is $\mathrm{IRF}(t)$, and vector $\boldsymbol{\varepsilon}$ is a residual term. The least-squares solution of the IRF $\mathbf{x}$ can be found by inverting $\mathbf{A}$. The

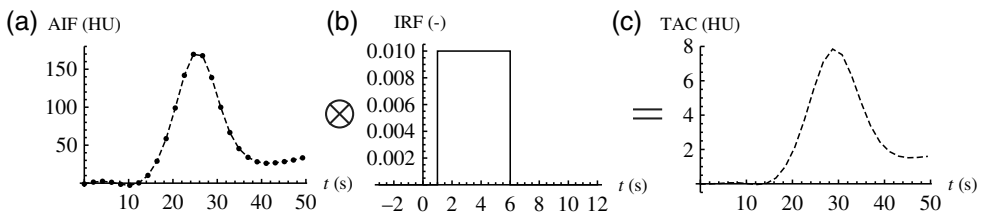

Fig. 1 (a) The measured AIF convolved with a computed estimate of the (b) IRF gives an estimate of the (c) TAC of the tissue.

bSVD method uses singular value decomposition (SVD) to find a pseudoinverse of **A**, which for circulant matrices is mathematically equivalent to applying a Fourier transform.

In order to suppress noise in the resulting IRF, the least significant eigenvectors are consecutively removed until **x** has an oscillation index below a certain threshold.[10] In this study, a threshold of 0.095 is used, as suggested by Wu et al.[11] The CBF is defined as the maximum value in the vector **x**. The CBV is estimated by calculating the ratio between the integrals of the measured TAC and the AIF.

The commercial method (Philips) is also SVD-based, but no detailed technical information about this algorithm is available. The code for the both the boxNLR method and the bSVD method was developed in-house; the bSVD method was implemented following the description of Wu et al.[11]

2.4 *Clinical Data*

Fifty consecutive patients were included retrospectively from a single center (University Medical Center Utrecht) participating in the Dutch acute stroke trial (DUST). The DUST study protocol has been described previously.[12] The DUST study was approved by the local institutional ethical review boards of the participating centers, and all patients or family gave signed informed consent.

CTP was performed on admission before possible thrombolytic treatment. All included scans were acquired on a 256-slice Philips Brilliance iCT scanner (Philips Healthcare, Best, The Netherlands) at 80 kVp and 150 mAs/rotation. The scans had a total acquisition time of about 50 s, divided into 25 frames with an ~2 s interval. This resulted in an effective radiation dose of 2.7 mSv. Before scanning, 40 mL of nonionic contrast agent (Ultravist 300, Bayer HealthCare, Berlin, Germany) was injected intravenously at a rate of 6 mL/s, followed by a 40-mL saline flush.

The scans had an axial coverage of 60 to 65 mm, covering the basal ganglia up to above the lateral ventricles. The scan volume was lowered if a posterior circulation stroke was suspected. The slices had a field-of-view of ~200 mm × 200 mm and a slice thickness of 5 mm, and were reconstructed in a 512 × 512 matrix using filtered backprojection, yielding a pixel size of 0.39 mm × 0.39 mm.

Prior to analysis, the scans were corrected for motion using a rigid registration method[13] and filtered using a bilateral filter.[14] This filter computes a bilateral weight based on the Euclidean distance between two voxels and the squared difference in average intensity between the TACs of those voxels. The spatial SD of the Gaussian kernel of this filter was 3 mm, and the intensity SD was 20 HU[2]. These settings resulted in similar noise levels as in the filtered phantom.

Whenever possible, an internal carotid artery was chosen to provide the AIF. If this location happened to be outside the imaged volume, a middle or anterior cerebral artery was chosen. VOFs were selected in the superior sagittal sinus or the transverse sinus near the torcular herophili. The same AIF and VOF locations were used for all three methods.

2.5 *Analysis*

All three analysis methods generated CBV, MTT, and CBF perfusion maps for the digital phantom and for the clinical data. It should be noted that, although three parameters were measured, these perfusion parameters capture just two degrees of freedom because of their interrelation: MTT = CBV/CBF. The area under the curve of the VOF was used to correct the CBV and CBF values for partial volume effects in the AIF. CBV and CBF values were furthermore corrected for the difference in hematocrit between large and small vessels.[15]

Similarly to the approach by Kudo et al., the average perfusion value in each tile was calculated by averaging all pixels in a 28 × 28 pixel region centered on each 32 × 32 pixel large tile.[7] In order to compare these measured values with the ground truth, linear fits through the origin and Pearson correlation coefficients (ρ) were calculated for the three IRF types separately, and for the IRF types combined. Good correlation was defined as $\rho > 0.9$. To check if the measurements conformed to the input values under ideal circumstances, the linear fits and correlation coefficients were also calculated on a noise-free version of the digital phantom.

To assess the effect of noise on the perfusion values, the phantom data were filtered with eight 2-D Gaussian filter kernels with decreasing radius. This resulted in eight increasing noise levels, ranging from 0.84 HU (SD) at a kernel size of 2.5 pixels (SD) to 2.3 HU at a kernel size of 0.93 pixels. At each noise level, Pearson coefficients of correlation with the ground truth were calculated, as well as the median and the interquartile range of the bias in average tile value as compared

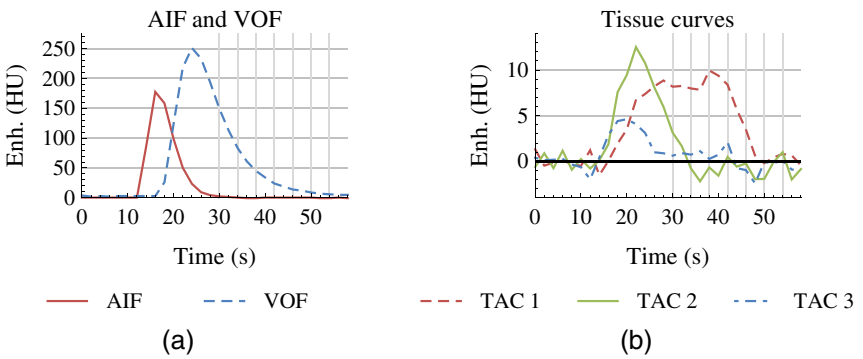

Fig. 2 Examples of attenuation curves. (a) The AIF and VOF measured in the filtered digital phantom. (b) Three enhancement curves measured in the tile with (1) a box-shaped IRF with CBV of 5 mL/100 g, MTT of 24 s, and 3.0 s delay, (2) a linear IRF with CBV of 3.0 mL/100 g, MTT of 6.0 s, and 1.5 s delay, and (3) an exponential IRF with CBV of 1 mL/100 g, MTT of 3.4 s, and no delay. The seven vertical gray lines, starting at 30 s, mark the time frames at which the curves were truncated.

with the lowest noise level. Pearson coefficients were calculated per IRF and then averaged.

The effect of truncation of the attenuation curves was assessed by truncating the phantom data from 58 to 30 s in steps of 4 s, i.e., two time frames of 2 s [vertical lines in Figs. 2(a) and 2(b)]. In each step, Pearson coefficients of correlation with the ground truth were calculated, as well as the median and interquartile range of the bias in average tile value as compared with data of 58 s duration. Again Pearson coefficients were calculated per IRF and then averaged.

For the analysis of the clinical data, bSVD was considered the reference method. The perfusion maps of the commercial method and of the boxNLR method were each compared with that obtained using bSVD. Linear fits through the origin and Pearson correlation coefficients were calculated per patient, using all parenchymal voxels. Mean CBF, CBV, and MTT values were calculated in the brain tissue in both the ipsilateral and the contralateral hemisphere. Symmetry lines were drawn manually to separate the hemispheres.

The time frames before bolus arrival, which is estimated by curve-fitting of the AIF, were averaged to obtain a noncontrast CT image. Only the voxels that had an average CT value >17 and <55 HU were classified as parenchymal tissue and included in the analysis. Voxels with a blood volume >9 mL/100 g were classified as vessels and excluded from the analysis.

3 Results

3.1 *Phantom Data*

Figure 3 shows an example of the ground truth and estimated perfusion maps of one of 2-D slices in the phantom. Although all three methods were supposed to be delay-insensitive, the perfusion maps of the commercial method and bSVD both showed diagonal bands in the CBF and MTT maps. Also, the response to high CBF and low MTT values seemed to be reduced for both methods. The commercial method furthermore showed overestimated CBV values.

The slopes and correlation coefficients of the average measurements with respect to the ground truth are given in Table 1 (phantom with noise). All methods showed good correlation with the ground truth for each of the three IRF shapes ($\rho > 0.90$). For the three IRF types combined, however, the Pearson coefficients for CBF measured with the commercial method and boxNLR were smaller than 0.9. The R^2 values and the correlation coefficients were highest for CBV and were comparable among the three methods. The bSVD and boxNLR methods showed higher R^2 values and correlation coefficients for CBF and MTT than the commercial method.

As a conformance test, the slopes and correlation coefficients of the average measurements in the noise-free phantom are given in Table 2. Both the bSVD and boxNLR methods show overall higher R^2 values and correlation coefficients. As expected, the slopes and R^2 values of the parameters measured with boxNLR on TACs with box-shaped IRFs are both close to 1. However, the commercial method unexpectedly showed elevated CBF and CBV values, and slightly worse correlation coefficients as compared to the values in Table 1.

3.2 *Response to Noise*

Figure 4 shows an example of the ground truth and estimated perfusion maps of one of 2-D slices in the phantom, filtered with a smaller 2-D Gaussian kernel (SD 0.93 pixels, versus 2.5 pixels for Fig. 3). This resulted in perfusion maps with a higher noise level than those in Fig. 3. The visual differences between maps of the same method in Figs. 3 and 4 were small. The CBV and MTT maps showed a rather uniform noise level throughout each slice, but the noise level of the CBF seemed to increase with the CBF value (top right map in Fig. 4).

As concerns correlation with the ground truth, all methods showed a similar trend in response to noise (Fig. 5). Only the MTT values showed a linear decrease in correlation as a function of the noise level, in roughly the same fashion for each of the methods [Fig. 5(c)].

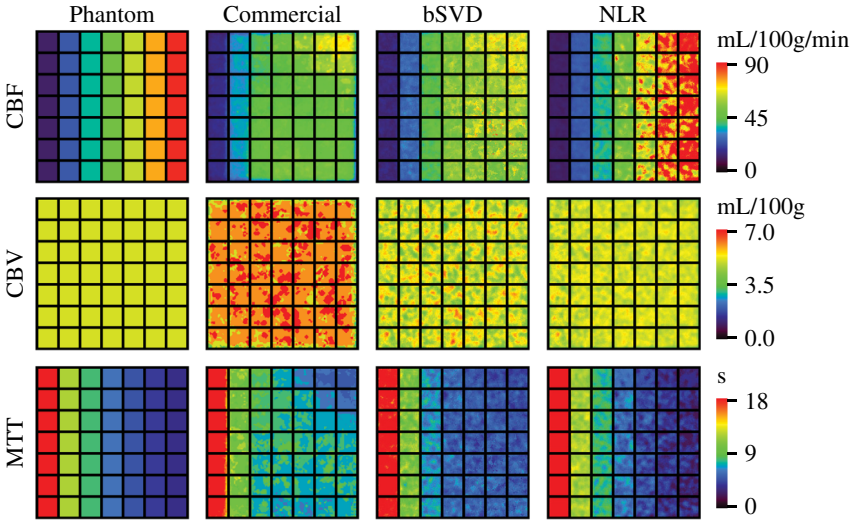

Fig. 3 Ground truth maps and measured perfusion maps of the last slice of the digital phantom, i.e., a box-shaped IRF and CBV of 5 mL/100 g. The phantom was filtered using a 2-D Gaussian kernel with an SD of 2.5 pixels. All tiles in this slice have the same box-shaped IRF and a CBV of 5 mL/100 g, while the MTT was varied horizontally (24 to 3.4 s, from left to right), and the tracer delay was varied vertically (0 to 3 s, from top to bottom). The CBF can be determined by the central volume principle: CBV = CBF × MTT.

Table 1 Phantom measurements with default noise level. Slope and goodness of fit (R^2) and Pearson correlation coefficient (ρ) for the relation between the measured perfusion values and the ground truth values of the phantom. The slopes and R^2 values were calculated for a linear fit through the origin. The values were measured for each IRF shape separately (exponential, linear, and box-shaped) as well as for the three shapes combined (All). The best fits and highest correlation coefficients are bold-faced.

		Slope (R^2)			Pearson ρ		
		Commercial method	bSVD	boxNLR	Commercial method	bSVD	boxNLR
Exponential	**CBF**	0.55 (0.84)	0.58 (0.93)	**0.47 (0.96)**	0.96	0.97	**0.98**
	CBV	1.12 (0.96)	**0.95 (0.96)**	0.86 (0.95)	0.98	**0.98**	0.97
	MTT	1.13 (−0.18)	1.02 (0.32)	**1.25 (0.59)**	**0.96**	0.96	0.93
Linear	**CBF**	0.66 (0.83)	0.71 (0.95)	**0.68 (0.98)**	0.95	0.98	**0.99**
	CBV	1.18 (0.98)	**0.98 (0.99)**	0.96 (0.99)	0.99	**1.00**	0.99
	MTT	1.09 (0.59)	0.99 (0.85)	**1.22 (0.90)**	0.98	**0.98**	0.97
Box-shaped	**CBF**	0.76 (0.69)	0.83 (0.85)	**1.12 (0.98)**	0.90	0.94	**0.99**
	CBV	1.20 (0.98)	0.99 (0.99)	**1.00 (1.00)**	0.99	1.00	**1.00**
	MTT	0.91 (0.51)	0.83 (0.85)	**0.96 (0.99)**	0.97	0.98	**0.99**
All	**CBF**	0.65 (0.72)	**0.71 (0.85)**	0.76 (0.71)	0.89	**0.93**	0.84
	CBV	1.17 (0.97)	**0.97 (0.98)**	0.94 (0.96)	0.98	**0.99**	0.98
	MTT	1.04 (0.34)	0.95 (0.68)	**1.14 (0.81)**	0.93	**0.94**	0.92

Table 2 Noise-free phantom measurements. Slope and goodness of fit (R^2) and Pearson correlation coefficient (ρ) for the relation between the measured perfusion values and the ground truth values of the noise-free phantom. The slopes and R^2 values were calculated for a linear fit through the origin. The values were measured for each IRF shape separately (exponential, linear, and box-shaped) as well as for the three shapes combined (All). The best fits and highest correlation coefficients are bold-faced.

		Slope (R^2)			Pearson ρ		
		Commercial method	bSVD	boxNLR	Commercial method	bSVD	boxNLR
Exponential	**CBF**	1.05 (0.85)	0.62 (0.96)	**0.41 (0.98)**	0.93	0.98	**0.99**
	CBV	2.01 (0.94)	**0.86 (0.98)**	0.82 (0.96)	0.97	**0.99**	0.98
	MTT	1.00 (0.12)	0.98 (0.75)	**1.40 (0.79)**	0.93	0.96	**0.99**
Linear	**CBF**	1.29 (0.84)	0.75 (0.98)	**0.61 (1.00)**	0.94	0.99	**1.00**
	CBV	2.13 (0.97)	0.89 (1.00)	**0.91 (0.99)**	0.99	**1.00**	0.99
	MTT	0.93 (0.64)	**1.01 (0.96)**	1.32 (0.98)	0.96	0.99	**1.00**
Box-shaped	**CBF**	1.47 (0.68)	0.87 (0.87)	**1.04 (0.97)**	0.88	0.94	**0.99**
	CBV	2.16 (0.97)	0.90 (1.00)	**0.93 (1.00)**	0.99	1.00	**1.00**
	MTT	0.78 (0.55)	0.85 (0.96)	**0.97 (0.99)**	0.94	0.99	**1.00**
All	**CBF**	1.27 (0.73)	**0.74 (0.87)**	0.69 (0.69)	0.88	**0.94**	0.83
	CBV	2.10 (0.96)	**0.89 (0.99)**	0.89 (0.97)	0.99	**0.99**	0.98
	MTT	0.90 (0.43)	**0.95 (0.88)**	1.23 (0.86)	0.91	**0.96**	0.94

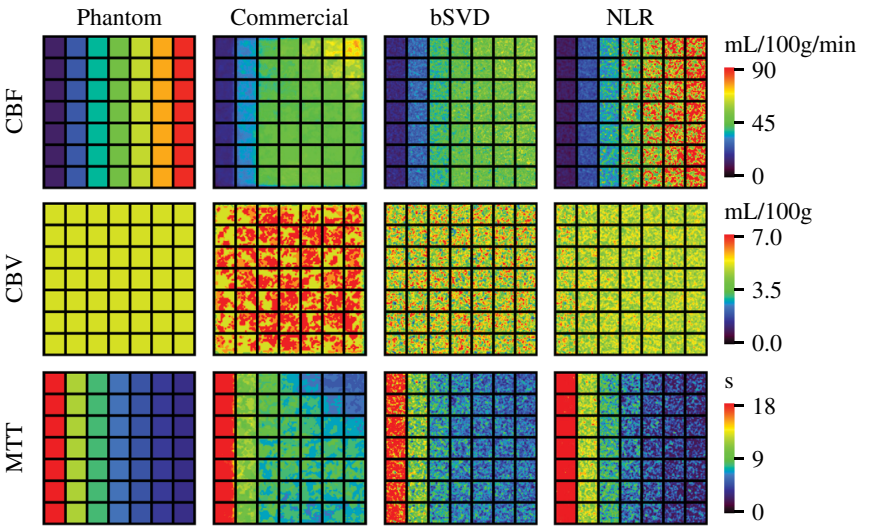

Fig. 4 Ground truth maps and measured perfusion maps in the same phantom slice as shown in Fig. 3. In this case, however, the phantom was filtered using a 2-D Gaussian filter with an SD of just 0.93 pixels, resulting in a higher noise level (noise SD = 2.3 HU).

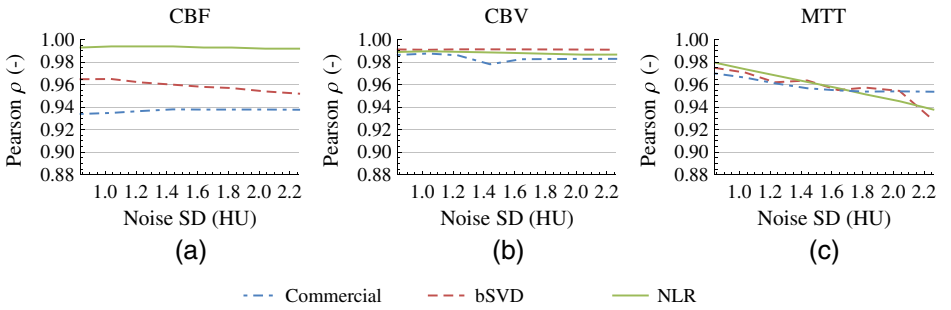

Fig. 5 Correlation with ground truth as a function of noise level: (a) CBF, (b) CBV, and (c) MTT. The figures show the Pearson coefficients of the correlation of the estimated perfusion values with the ground truth in the phantom, as a function of the noise level.

The bias with respect to the low-noise maps as a function of noise level (Fig. 6) differed substantially among the three methods. Median CBF measured with the commercial method and with boxNLR increased with the noise level, but decreased when measured with bSVD. Median CBV values measured with bSVD and boxNLR were not strongly influenced by noise, but CBV values measured with the commercial method increased with noise level. Median MTT measured with boxNLR showed no bias due to noise, but increased with noise when measured with the commercial method and with bSVD.

3.3 *Response to Truncation*

The commercial and bSVD methods gave visually similar responses to truncation of attenuation curves, as is shown in Fig. 7. The boxNLR method showed the smallest differences with the analysis on the full curves (Fig. 3). The estimates in

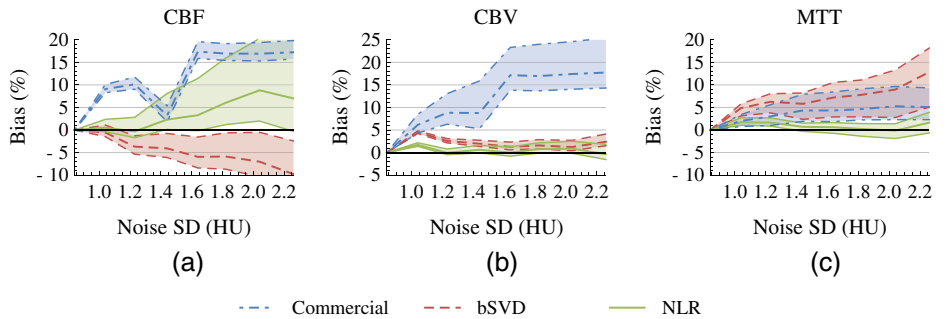

Fig. 6 Bias of the perfusion analysis methods due to noise: (a) CBF, (b) CBV, and (c) MTT. The figures show the median and interquartile ranges of the bias of the estimated perfusion values to low-noise estimates, as a function of noise level.

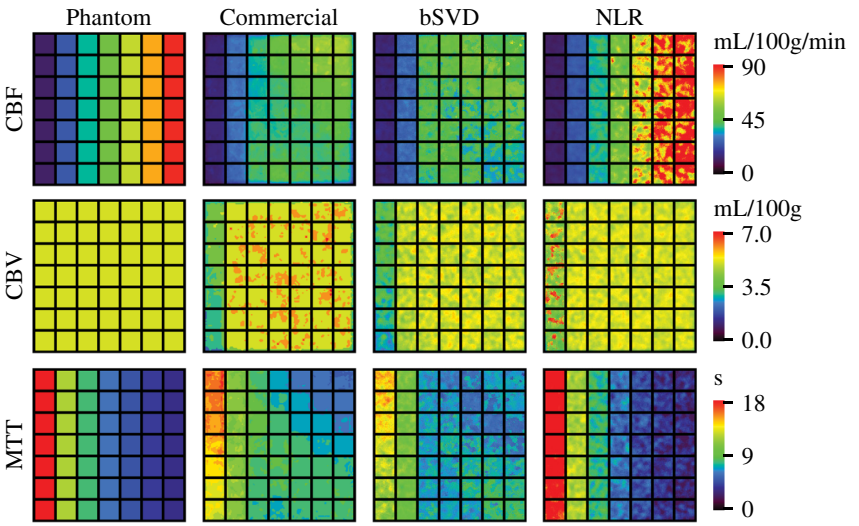

Fig. 7 Ground truth maps and measured perfusion maps in the same phantom slice as shown in Fig. 3. In this case, however, just 18 out of 30 time frames (34 s) were analyzed, resulting in truncated attenuation curves [Fig. 2(b)]. The phantom was filtered using a 2-D Gaussian filter with an SD of 2.5 pixels.

the first row (MTT = 24 s) were the most affected by truncation, resulting in underestimated CBV values for the commercial and bSVD methods, and increased noise in CBV values for the boxNLR method.

The boxNLR method correlated better with the ground truth than the commercial method and bSVD (Fig. 8), especially when large numbers of frames were removed. The Pearson coefficients of the commercial method and bSVD showed similar trends.

As for bias of the TACs owing to truncation: the bSVD method showed a negative bias in CBF and CBV as a result of truncation, the boxNLR method seems to have no bias in either of the parameters, and the commercial method showed rather irregular biases as a function of the number of removed frames (Fig. 9). When 14 frames were removed, the commercial method failed to estimate the area under the VOF, for which reason the CBF and CBV were overestimated by 42% and 27%, respectively.

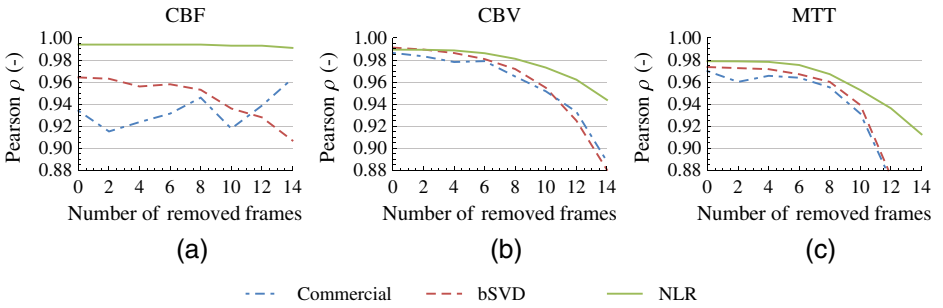

Fig. 8 Correlation with ground truth as a function of truncation level: (a) CBF, (b) CBV, and (c) MTT. The figures show the Pearson coefficients of the correlation of the estimated perfusion values with the ground truth in the phantom versus the number of removed frames.

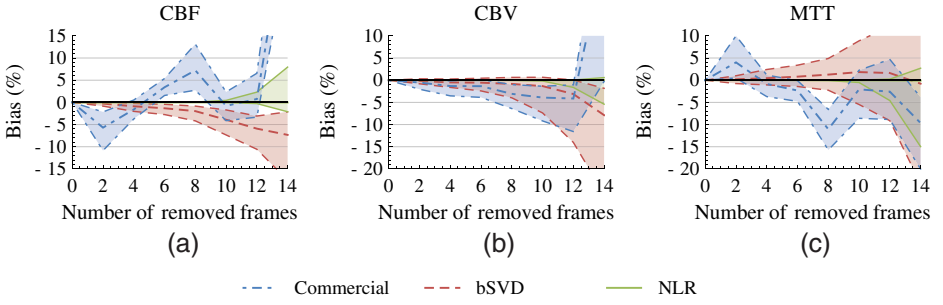

Fig. 9 Bias of the perfusion analysis methods due to truncation: (a) CBF, (b) CBV, and (c) MTT. The figures show the median and interquartile ranges of the bias of estimated perfusion values to the estimates without removed frames, as a function of the number of removed frames.

3.4 *Clinical Data*

Although the commercial method and bSVD were about five times faster than boxNLR, all three methods were able to analyze single clinical CTP slices within a second on a high-end desktop computer, and are therefore fast enough for clinical use.

Figure 10 shows an example of three boxNLR perfusion maps of clinical data, as well as a delay map. Note that both SVD methods are unable to provide delay estimates, although such estimates may contain relevant physiological information on, e.g., collateral flow. The slopes and Pearson coefficients of the correlation of the commercial method and boxNLR with the bSVD standard are given in Table 3, along with the ipsilateral and contralateral perfusion values.

The boxNLR method provided higher correlation with bSVD than the commercial method in all cases. There were, however, considerable differences among the average perfusion values measured by the three methods. The CBF values measured

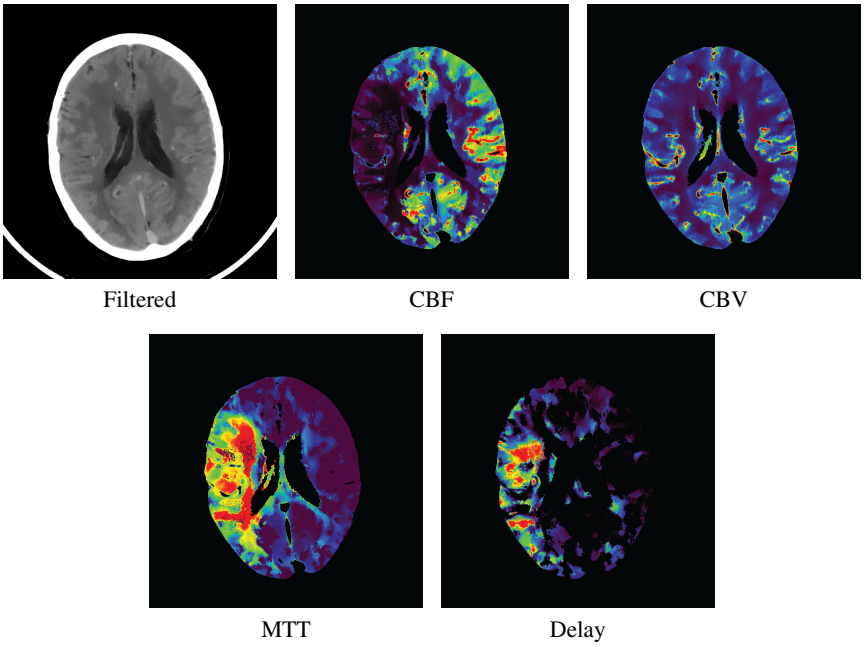

Fig. 10 Axial slice of a filtered clinical CTP image (5-mm slice thickness) and its CBF, CBV, MTT, and delay maps. These maps were generated using the model-based method (boxNLR).

Table 3 Slopes and Pearson coefficients of the correlation of the commercial and boxNLR methods with the bSVD standard, and the ipsilateral and contralateral CBF (mL/100 g/ min), CBV (mL/100 g), and MTT (s). The presented values are medians of the 50 CTP scans, with interquartile ranges between brackets.

		Commercial method	bSVD	boxNLR
Linear correlation with bSVD: Slope	**CBF**	1.55 (1.37, 1.83)	1	2.34 (1.92, 2.65)
	CBV	1.38 (1.22, 1.53)	1	1.06 (1.02, 1.09)
	MTT	0.97 (0.85, 1.09)	1	0.74 (0.54, 0.82)
Linear correlation with bSVD: Pearson ρ	**CBF**	0.66 (0.56, 0.76)	1	0.80 (0.76, 0.84)
	CBV	0.73 (0.69, 0.75)	1	0.99 (0.99, 0.99)
	MTT	0.51 (0.39, 0.76)	1	0.65 (0.54, 0.76)
Ipsi-lateral value	**CBF**	34.5 (23.9, 41.5)	23.0 (15.5, 26.2)	44.8 (28.7, 60.7)
	CBV	3.70 (3.08, 4.29)	2.62 (2.05, 3.11)	2.85 (2.01, 3.37)
	MTT	8.33 (6.85, 10.1)	8.00 (7.23, 8.76)	6.27 (4.11, 7.95)
Contra-lateral value	**CBF**	38.1 (28.1, 50.9)	24.9 (16.3, 29.6)	57.2 (37.1, 74.0)
	CBV	3.77 (2.98, 4.45)	2.70 (2.08, 3.14)	2.88 (1.93, 3.39)
	MTT	6.30 (5.58, 7.33)	7.01 (6.34, 7.72)	3.71 (3.22, 4.63)

with boxNLR were >2 times as high as measured with bSVD, and those measured with the commercial method 1.5 times as high. CBV values were comparable between boxNLR and bSVD inasmuch as both the slope and correlation coefficient were close to 1. The CBV values measured with the commercial method were 1.4 times higher than those measured with bSVD. The average MTT values were comparable between the commercial method and bSVD, although the correlation coefficients were low. The MTT values measured with boxNLR were lower than those measured with bSVD.

4 Discussion

This study has demonstrated that the proposed model-based method for CT brain perfusion analysis competes with current commercial and academic state-of-the-art methods. The method was found to be robust to noise, to truncation, and to tracer delay.

4.1 *Phantom Data*

The commercial method, boxNLR, and bSVD all showed high Pearson correlation coefficients with the ground truth ($\rho > 0.9$).

Both being SVD-based, the commercial method and bSVD showed perfusion maps with visually similar trends. Both methods underestimated CBF values and overestimated MTT values in hyperperfused areas, i.e., at the right side of the phantom. It is likely that this occurred because of regularization (smoothing) of the IRF, which decreased the amplitude. The responses of the boxNLR method were more linear, which is reflected by the higher R^2 values for the linear fits.

All methods, but boxNLR in particular, showed that the perfusion values measured in the phantom were dependent on IRF shape. It was found that when the distribution of transit times in the IRF becomes wider (the exponential IRF having the widest distribution and the box-shaped IRF the smallest), the estimated CBF values decreased and MTT values increased. For both SVD-based methods, this is most likely the result of the SVD regularization, which decreases the amplitude of the IRF as described above, whereas for the model-based method this is caused by the underlying model assuming a flat, box-shaped IRF.

The conformance test with the noise-free phantom confirmed that the boxNLR method provides relatively accurate, quantitative results with a matched, box-shaped IRF. For unknown reasons, the commercial method showed elevated CBF and CBV values and slightly worse correlation coefficients as compared to the phantom with default noise level.

4.2 *Response to Noise*

The effect of noise on the correlation of the perfusion maps with the ground truth was similar for all methods. The bias of the median perfusion values due to noise exhibited different trends, however, owing to fundamental differences between boxNLR and the SVD-based methods.

The boxNLR method showed a positive bias on CBF, but no bias on CBV and MTT. This can be explained by the fact that it is difficult to estimate high flow values since the dispersed AIF acts as a low-pass filter that limits temporal resolution. The noise on CBF therefore increases with increasing CBF (note that $\mathrm{CBF} = \mathrm{CBV}/\mathrm{MTT}$), which results in a skewed distribution and a positive bias.

The commercial method and bSVD, both SVD-based, apply adaptive regularization to suppress noise in the IRF. An increased noise level requires stronger smoothening of the IRF, resulting in a wider curve with lower amplitude, i.e., higher MTT and lower CBF. For this reason both methods showed a positively biased median MTT due to noise. The bSVD method furthermore showed a negatively biased CBF. The CBF of the commercial method was, however, positively biased due to the overestimated CBV.

In SVD-based deconvolution, the adaptive regularization needs to be tuned such that the deconvolved IRF matches the true IRF as close as possible. In model-based methods, however, putting in additional prior knowledge is not necessary, since the shape of the IRF is fully determined by the model. SVD-based deconvolution furthermore requires additional methods for extracting the CBF and CBV from the IRF (or from the AIF and TAC). In model-based methods, this is all unified in the model. These models can even be extended to also include other perfusion parameters, such as vascular permeability for predicting hemorrhagic transformation.[8,16] These advantages of model-based methods may lead to smaller variability in results due to differences in implementations, or differences in data properties such as temporal resolution or noise level.

Although all three methods showed biased CBF values due to noise, the impact of these biases in clinical applications will probably be moderate. As discussed above, the biases are most significant in the hyperperfused (healthy) areas, and are therefore unlikely to affect tissue classification.

4.3 *Response to Truncation*

It was found that the boxNLR method was more robust to truncation than the commercial and bSVD methods, since it yielded perfusion values with higher correlation to the ground truth, and no bias in median value due to truncation. Whereas the SVD-based methods do not assume a model, the box-shaped IRF model used by the model-based method allows extrapolation of the truncated curves, resulting in unbiased estimates.

It was unclear why the commercial method showed a rather irregular bias in CBF and MTT due to truncation.

The commercial method furthermore showed severely overestimated CBV and CBF values at a 14-frame truncation of the TAC. This was caused by erroneous curve-fitting of the truncated VOF.

4.4 *Clinical Data*

With respect to the clinical scans, the boxNLR perfusion maps showed higher correlation with bSVD than the maps generated by the commercial clinical software.

The CBF estimates in the 50 perfusion scans were more than two times higher when measured with the boxNLR method than measured with the bSVD method, and were also higher than measured with the commercial method. This large difference can be explained by the opposite biases due to noise found in the phantom study, and also by the difference in slope as measured with the box-shaped phantom IRF (Table 1). This suggests that the physiological IRF mostly resembles this box-shape, which is supported by simulations published by Bredno et al., and assumed in many tracer-kinetic models for tissue perfusion.[17–20]

MTT values measured with boxNLR were lower than those measured with bSVD. This is also in line with the biases due to noise as found in the phantom study.

The commercial method showed higher CBV values than bSVD and boxNLR in the 50 perfusion scans, as well as elevated CBV values with respect to the ground truth in the perfusion phantom. Possible explanations are differences in hematocrit correction or in curve fitting of the AIF and VOF.

Although ground truth perfusion values for the clinical scans were not available, which is a limitation of this study, highly quantitative Xe-CT and ^{15}O-PET studies confirmed average literature CBF values of about 50 mL/100 g/min and average transit times of about 3 to 5 s in the healthy hemisphere (gray and white matter combined).[21–23] The boxNLR method provided better matching values (57 mL/100 g/min and 3.7 s) than the commercial method (38 mL/100 g/min and 6.3 s) and bSVD (25 mL/100 g/min and 7.0 s). A previous study also reported that bSVD underestimates quantitative CBF values, presumably due to image noise.[24]

More quantitative methods could lower the variability in CTP measurements due to observers, scanners, acquisition protocols, reconstruction methods, and analysis software. This may in turn result in more robust predictions of infarct core and penumbra, and minimizing the need for situation-specific thresholds and other software-calibration.[25] Since the prediction of these regions is the major application of CTP imaging in stroke, further study into the effects on infarct core and penumbra prediction is desired.

4.5 *Limitations*

This study has other limitations besides the lack of ground truth clinical perfusion values as mentioned in the previous paragraph. Although the IRF of cerebral tissue is frequently modeled as a box function, the true physiological shape is unknown. To our knowledge no accurate IRF has ever been measured with high resolution. The phantom study showed, however, that the investigated methods all correlated well with the ground truth, regardless of the IRF shape used.

Although all major CT manufacturers provide CTP analysis software, Philips EBW was used mainly because of institutional availability. However, the vast majority of all commercial programs are based on similar SVD-like inverse filtering as the Philips algorithm, and Kudo et al. found that the academic bSVD method showed better correlations with the ground truth than all commercial software tested, including the Philips Software.[7] Although further research is required, it may therefore be hypothesized that as the boxNLR method performed equally or better than the academic bSVD method, it will also perform equally or better than other commercial software.

It should also be noted that the commercial method uses a different curve fitting algorithm for partial volume correction than the boxNLR and bSVD methods. This means that the differences in CBV and CBF might have been influenced by the robustness of curve fitting, especially in the case of the truncated VOF curves. MTT values are not changed by partial volume correction.

5 Conclusion

Being model-independent, i.e., independent of an assumption of IRF shape, is often presented as an advantage of SVD-based methods. This study showed, however, that the use of a tracer kinetic model has some striking advantages over SVD-based methods. Least-squares fitting of the IRF model provides improved robustness to attenuation curve truncation, extensibility, and unified estimation of perfusion parameters. However, since the clinically used thresholds were established on perfusion estimates that were most likely biased, they cannot be applied to perfusion maps generated by a different method and may therefore need revision.

In conclusion, the proposed boxNLR method provides a fast and reliable way of estimating perfusion parameters from CTP scans. This suggests it could be a viable alternative to the current commercial and academic perfusion analysis methods.

Appendix: MATLAB Implementation of the boxNLR Method

The following lines give an example of a basic MATLAB implementation of the nonlinear regression CTP analysis method as described in the methods section. Ideally, the shifted versions of `auc` (the integrand of the AIF), i.e. variables `a` and `b`, should be calculated by convolving the AIF with the integral of a suited interpolation kernel. However, by using a cumulative sum and linear interpolation instead of convolution, this approximation is both faster and simpler.

```
% Estimate the perfusion parameters (x;
% CBV, MTT, and delay) that explain the
% tissue signal (tac) resulting from the
% input signal (aif). dt is the sample
% interval.
function x = boxnlr(aif, tac, dt)

% Initial estimates for CBV, MTT, and
% delay, respectively. Divide MTT and
% delay by dt seconds to convert to
% unitless values.
x0 = [0.05; 4/dt; 1/dt];

% Convolve AIF and TAC with a 3-point
% bandlimiting kernel with a FWHM of
% 2 samples. Handle edges by nearest
% neighbor extrapolation.
k = [0.25; 0.5; 0.25];
aif_k = conv([aif(1);aif;aif(end)], ...
    k, 'valid');
tac_k = conv([tac(1);tac;tac(end)], ...
    k, 'valid');

% Calculate the numerical integrand of
% the bandlimited AIF. Note that this
% cumulative sum introduces a half
% sample shift.
auc = cumsum(aif_k);

% Find optimal values. Fminsearch
% requires the MATLAB Optimization
% Toolbox. By default the method uses a
% Nelder-Mead simplex algorithm with a
% step size of 5% of the initial value.
f = @(x) fun(x, auc, tac_k);
x = fminsearch(f, x0);
```

```
% Multiply MTT and delay by dt seconds
% to convert from unitless values.
x = [x(1); x(2)*dt; x(3)*dt];

% Calculate the sum of squared errors
% (sse) between the measured TAC and the
% TAC generated from the AIF using the
% perfusion parameters in x.
function sse = fun(x, auc, tac_k)
tac_est = gen_tac(x(1)/x(2), x(2), ...
    x(3), auc);
sse = sum((tac_est - tac_k).^2);

% Generate a TAC from the AIF and a set
% of perfusion parameters. When a box-
% shaped impulse response is assumed,
% then the TAC can be calculated as the
% difference of shifted integrands of
% AIF. Note that an additional half
% sample shift is required to correct
% for the shift introduced by the
% cumulative sum. In case negative
% shifts should be handled correctly,
% then interp1 needs to extrapolate the
% right side of the integrated AIF.
function tac = gen_tac(cbf, mtt, d, auc)
n = length(auc);
a = interp1(auc, (1:n)'-0.5-d, ...
   'linear', 0);
b = interp1(auc, (1:n)'-0.5-d-mtt, ...
   'linear', 0);
tac = cbf * (a - b);
```

Acknowledgments

This work was supported by a research grant from the Dutch Technology Foundation STW (AIRSPACE, 11632). The project AIRSPACE received in-kind funding from Philips Healthcare and the LifeTec Group. The CTP data were collected under the Dutch Acute Stroke Trial (DUST, clinicaltrials.gov ID NCT00880113). The DUST study was funded by the University Medical Center Utrecht, The Netherlands Heart Foundation (2008T034), the NutsOhra Foundation (0903-012), and in-kind by Philips Healthcare. The funders had no role in study design, data collection and analysis, decision to publish, or preparation of the article.

References

1. K. Kudo et al., "Difference in tracer delay-induced effect among deconvolution algorithms in CT perfusion analysis: quantitative evaluation with digital phantoms," *Radiology* **251**(1), 241–249 (2009).
2. K. Kudo et al., "Differences in CT perfusion maps generated by different commercial software: quantitative analysis by using identical source data of acute stroke patients," *Radiology* **254**(1), 200–209 (2010).
3. L. Østergaard et al., "High resolution measurement of cerebral blood flow using intravascular tracer bolus passages. part I: mathematical approach and statistical analysis," *Magn. Reson. Med.* **36**(5), 715–725 (1996).
4. L. Østergaard et al., "High resolution measurement of cerebral blood flow using intravascular tracer bolus passages. Part II: experimental comparison and preliminary results," *Magn. Reson. Med.* **36**(5), 726–736 (1996).
5. J. Borst et al., "Effect of extended CT perfusion acquisition time on ischemic core and penumbra volume estimation in patients with acute ischemic stroke due to a large vessel occlusion," *PloS One* **10**(3), e0119409 (2015).
6. A. Konstas et al., "Theoretic basis and technical implementations of CT perfusion in acute ischemic stroke, part 2: technical implementations," *Am. J. Neuroradiol.* **30**(5), 885–892 (2009).
7. K. Kudo et al., "Accuracy and reliability assessment of CT and MR perfusion analysis software using a digital phantom," *Radiology* **267**(1), 201–211 (2013).
8. E. Bennink et al., "A fast nonlinear regression method for estimating permeability in CT perfusion imaging," *J. Cereb. Blood Flow Metab.* **33**, 1743–1751 (2013).
9. K. Nambu, R. Takehara, and T. Terada, "A method of regional cerebral blood perfusion measurement using dynamic CT with an iodinated contrast medium," *Acta Neurol. Scand.* **93**(s166), 28–31 (1996).
10. G. Gobbel and J. Fike, "A deconvolution method for evaluating indicator-dilution curves," *Phys. Med. Biol.* **39**(11), 1833 (1994).
11. O. Wu et al., "Tracer arrival timing-insensitive technique for estimating flow in MR perfusion-weighted imaging using singular value decomposition with a block-circulant deconvolution matrix," *Magn. Reson. Med.* **50**(1), 164–174 (2003).
12. T. van Seeters et al., "Prediction of outcome in patients with suspected acute ischaemic stroke with CT perfusion and CT angiography: the Dutch acute stroke trial (DUST) study protocol," *BMC Neurol.* **14**(1), 37 (2014).
13. S. Klein et al., "Elastix: a toolbox for intensity-based medical image registration," *IEEE Trans. Med. Imaging.* **29**(1), 196–205 (2010).
14. C. Tomasi and R. Manduchi, "Bilateral filtering for gray and color images," in *Sixth Int. Conf. on Proc. Computer Vision*, pp. 839–846, IEEE (1998).
15. A. A. Konstas et al., "Theoretic basis and technical implementations of CT perfusion in acute ischemic stroke, part 1: theoretic basis," *Am. J. Neuroradiol.* **30**(4), 662–668 (2009).
16. E. Bennink et al., "CT perfusion analysis by nonlinear regression for predicting hemorrhagic transformation in ischemic stroke," *Med. Phys.* **42**, 4610–4618 (2015).
17. J. Bredno, M. E. Olszewski, and M. Wintermark, "Simulation model for contrast agent dynamics in brain perfusion scans," *Magn. Reson. Med.* **64**(1), 280–290 (2010).
18. T. Koh et al., "A physiologic model of capillary-tissue exchange for dynamic contrast-enhanced imaging of tumor microcirculation," *IEEE Trans. Biomed. Eng.* **50**(2), 159–167 (2003).
19. K. B. Larson, J. Markham, and M. E. Raichle, "Tracer-kinetic models for measuring cerebral blood flow using externally detected radiotracers," *J. Cereb. Blood Flow Metab.* **7**(4), 443–463 (1987).
20. S. P. Sourbron and D. L. Buckley, "Tracer kinetic modelling in MRI: estimating perfusion and capillary permeability," *Phys. Med. Biol.* **57**, R1–R33 (2012).
21. M. Ibaraki et al., "Cerebral vascular mean transit time in healthy humans: a comparative study with PET and dynamic susceptibility contrast-enhanced MRI," *J. Cereb. Blood Flow Metab.* **27**(2), 404–413 (2007).
22. M. Wintermark et al., "Simultaneous measurement of regional cerebral blood flow by perfusion CT and stable xenon CT: a validation study," *Am. J. Neuroradiol.* **22**(5), 905–914 (2001).
23. H. Yonas et al., "CBF measured by Xe-CT: approach to analysis and normal values," *J. Cereb. Blood Flow Metab.* **11**(5), 716–725 (1991).
24. M. Sasaki et al., "Tracer delay-insensitive algorithm can improve reliability of CT perfusion imaging for cerebrovascular steno-occlusive disease: comparison with quantitative single-photon emission CT," *Am. J. Neuroradiol.* **30**(1), 188–193 (2009).
25. M. Wintermark et al., "Acute stroke imaging research roadmap II," *Stroke* **44**(9), 2628–2639 (2013).

Biographies for the authors are not available.